

Article

Effects of Astronomical Cycles on Laminated Shales of the Paleogene Shahejie Formation in the Dongying Sag, Bohai Bay Basin, China

Qiqi Li ¹ , Shang Xu ^{2,*}, Junliang Li ³, Ruichao Guo ³, Guangwei Wang ^{2,*} and Yufan Wang ¹

¹ Key Laboratory of Tectonics and Petroleum Resources, Ministry of Education, China University of Geosciences, Wuhan 430074, China

² Shandong Provincial Key Laboratory of Deep Oil & Gas, China University of Petroleum (East China), Qingdao 266580, China

³ Exploration and Development Research Institute of Shengli Oilfield, Sinopec, Dongying 257000, China

* Correspondence: xushang0222@163.com (S.X.); wanggw@upc.edu.cn (G.W.)

† Current Address: School of Geosciences, China University of Petroleum, Qingdao 266580, China.

Abstract: Laminated shales are widely developed in the Dongying Sag and have attracted much attention as an oil reservoir. Macroscopically, these shales generally have multi-scale cyclicity, which is closely related to the development of laminae. Therefore, analyzing the origin of their cyclicity is helpful to understanding the formation mechanism of laminated shales and the vertical heterogeneity of shale reservoirs, which are of great significance for continental shale oil exploration and development. In this study, a gamma ray (GR) logging series, high-resolution elemental geochemical data, high-resolution core scanning photos and grayscale data, and mineralogical data were used to characterize the cyclicity of shale at different scales, and their relationship with different astronomical cycles was discussed. The results show that the Es3L and Es4U shale in the Dongying Sag has cyclicity from the meter-scale to the ten-meter scale and then to the hundred-meter scale, which is mainly manifested by periodic changes in organic matter abundance, mineral composition, element abundance, and grayscale. These cycles of different scales coincide with different astronomical periods. Specifically, the hundred-meter scale cyclicity is mainly controlled by the very long orbital period; the ten-meter scale cyclicity is mainly related to the eccentricity cycle; while the precession period is the main driver of the meter-scale cyclicity. Finally, we propose a simplified model for illustrating the formation of rhythmic organic-rich shale. This study is helpful to understanding the origin of continental organic-rich shale and predicting shale reservoir properties.

Keywords: organic-rich shale; astronomical forcing; laminated shale; shale oil; Bohai Bay Basin



Citation: Li, Q.; Xu, S.; Li, J.; Guo, R.; Wang, G.; Wang, Y. Effects of Astronomical Cycles on Laminated Shales of the Paleogene Shahejie Formation in the Dongying Sag, Bohai Bay Basin, China. *Energies* **2023**, *16*, 3624. <https://doi.org/10.3390/en16093624>

Academic Editor: Mofazzal Hossain

Received: 7 March 2023

Revised: 10 April 2023

Accepted: 19 April 2023

Published: 23 April 2023



Copyright: © 2023 by the authors. Licensee MDPI, Basel, Switzerland. This article is an open access article distributed under the terms and conditions of the Creative Commons Attribution (CC BY) license (<https://creativecommons.org/licenses/by/4.0/>).

1. Introduction

Laminae are the thinnest sedimentary layer in sedimentary rocks. As the smallest units in shale oil enrichment, they have aroused interest among global geologists. The origin of laminae remains a mystery, and in most cases, they are considered as annual sedimentary cycles. However, macroscopically, laminated shales generally have multi-scale cyclicity, which is closely related to the development of laminae. Therefore, analyzing the origin of cyclicity is helpful to understanding the formation mechanism of laminated shales.

Cyclicity with different scales has been recorded in various types of sedimentary rocks in many basins around the world [1–3]. The explanation of its genesis can be summarized by several mechanisms, including orbital forcing [3,4], local basin dynamics [5], and material redistribution caused by diagenesis [6]. In recent years, with the continuous breakthroughs of shale oil and gas exploration and development, the origin of organic-rich shale has aroused great interest [7–9]. Current research suggests that shale is not as homogeneous as previously thought, but rather it is much more complex than any other sedimentary

rock, such as its strong heterogeneity [10,11]. Moreover, continental shale usually has a higher degree of heterogeneity than marine shale, which is mainly due to the small scale of the lake basin making it sensitive enough to respond to high-frequency environmental changes. As the vertical heterogeneity of shale reservoirs has an important impact on shale oil accumulation characteristics and hydraulic fracturing, many scholars have conducted extensive research on its control factors [3,4].

Studies have shown that changes in Earth's orbital parameters will control the distribution and intensity of insolation, resulting in periodic climate fluctuations on a timescale of 10,000 years to a million years [12,13], and thus directly or indirectly affect Earth-surface systems, such as weathering, sediment transport, and sedimentation [13]. Therefore, astronomical cycle signals have usually been recorded in lacustrine systems, which are sensitive to climate change [14–16]. Previous studies have focused on meter-scale cyclicity [3,17], but continental shale has cyclicity on multiple scales. However, multi-scale cyclicity has not been systematically analyzed and its controlling factors are still unclear.

The main aims of this paper are: (i) to characterize the cyclicity of Es3L and Es4U shale in the Dongying Sag at different scales and (ii) to elucidate the relationships between astronomically forced climate cycles and multi-scale cyclicity of shale.

2. Geological Setting

The Dongying Sag is a secondary structural unit of the Jiyang Depression in the Bohai Bay Basin and one of the typical hydrocarbon-rich sags in eastern China (Figure 1A). This sag is bordered by the Chenjiashuang Rise to the north, the Luxi Uplift and the Guangrao Rise to the south, the Binxian Rise and Qingcheng Rise to the west, and the Qingtuozi Rise to the east, with a total area of about 5700 km². The Dongying Sag is composed of several secondary structural units, including the Boxing Sub-sag, Lijin Sub-sag, Niuzhuang Sub-sag, Minfeng Sub-sag, the central anticline belt, north steep slope belt, and south slope belt (Figure 1A).

The Dongying Sag is a typical asymmetric half-graben lake basin, with a steep slope in the north and west controlled by faults and a gentle slope in the south and east (Figure 1B). The Chennan Fault in the north and the Pingnan Fault and Gaoqing Fault in the west are the main boundary faults, which control the evolution of the lake basin. The tectonic evolution of the Dongying Sag can be divided into two stages: the synrift stage (Figure 2) (65–24.6 Ma) and postrift stage (24.6 Ma–present) [18,19]. The synrift sequence unconformably overlies the Mesozoic strata and consists of the Paleogene Kongdian Formation (Ek), Shahejie Formation (Es), and Dongying Formation (Ed), which are mainly deposited in lacustrine environments. The postrift sequence is composed of the Neogene Guantao Formation (Eg) and Minhuazhen Formation (Em) and is mainly deposited in alluvial and fluvial environments (Figure 2) [18].

The Es formation is composed of sandstone, siltstone, mudstone, and evaporate, which can be subdivided into four members from top to bottom: Es1, Es2, Es3, and Es4. Of these, the Es3 Member can be further divided into Upper Es3 (Es3U), Middle Es3 (Es3M), and Lower Es3 (Es3L) intervals, and the Es4 Member can be further divided into Upper (Es4U) and Lower (Es4L) intervals (Figure 2). Our study target is the Es3L and the Es4U, which were formed during the expansion period of the lake. During this period, the high organic productivity and anoxic conditions of the bottom water resulted in the deposition of organic-rich shale with a thickness of ~400 m in the Es3L and Es4U [20]. They are not only important sources of rocks in the basin but also the target layers for shale oil exploration.

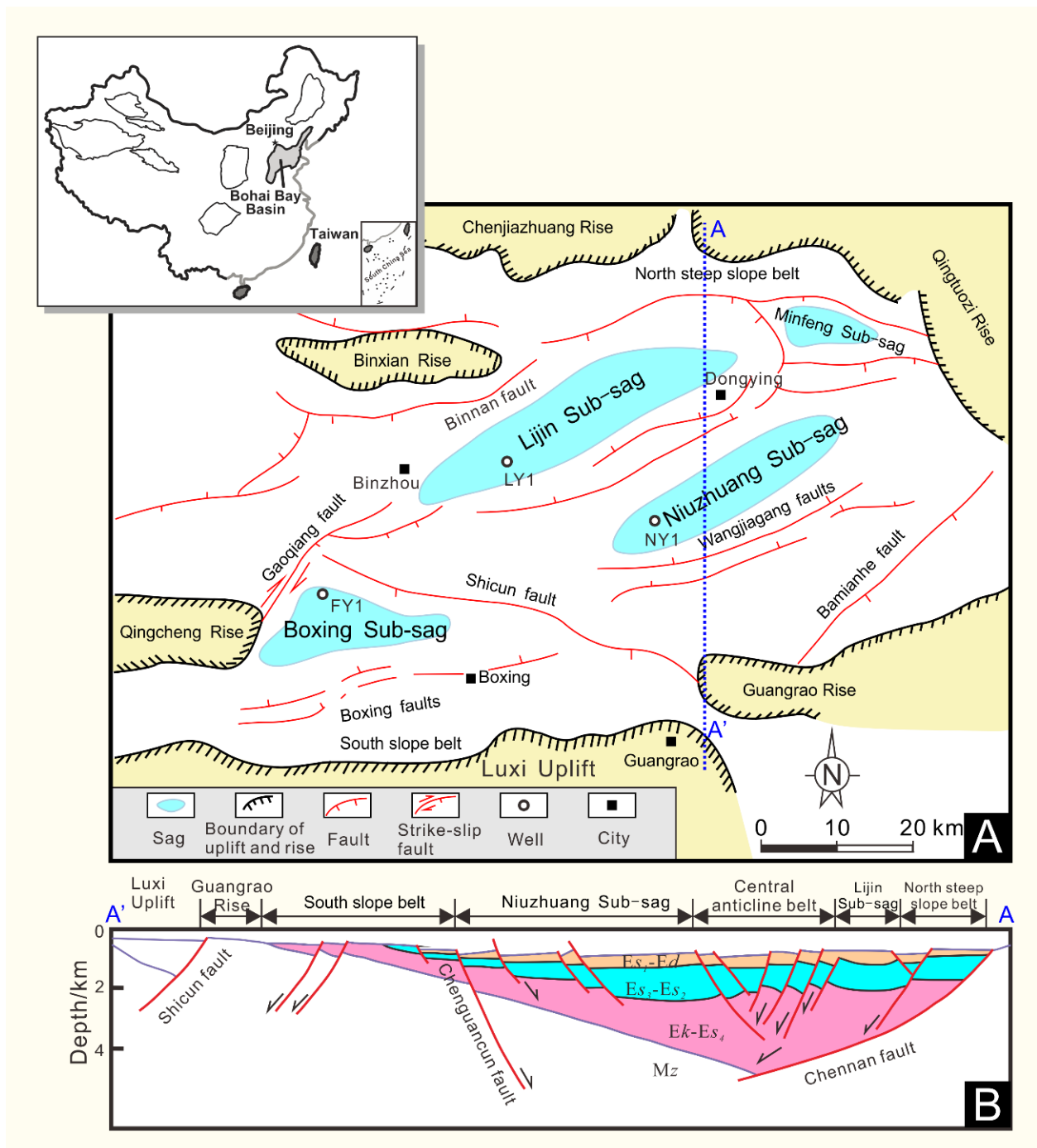


Figure 1. (A) The location of the Dongying Sag and its tectonic units. (B) Cross section showing the structural framework of the Dongying Sag (modified from [18]).

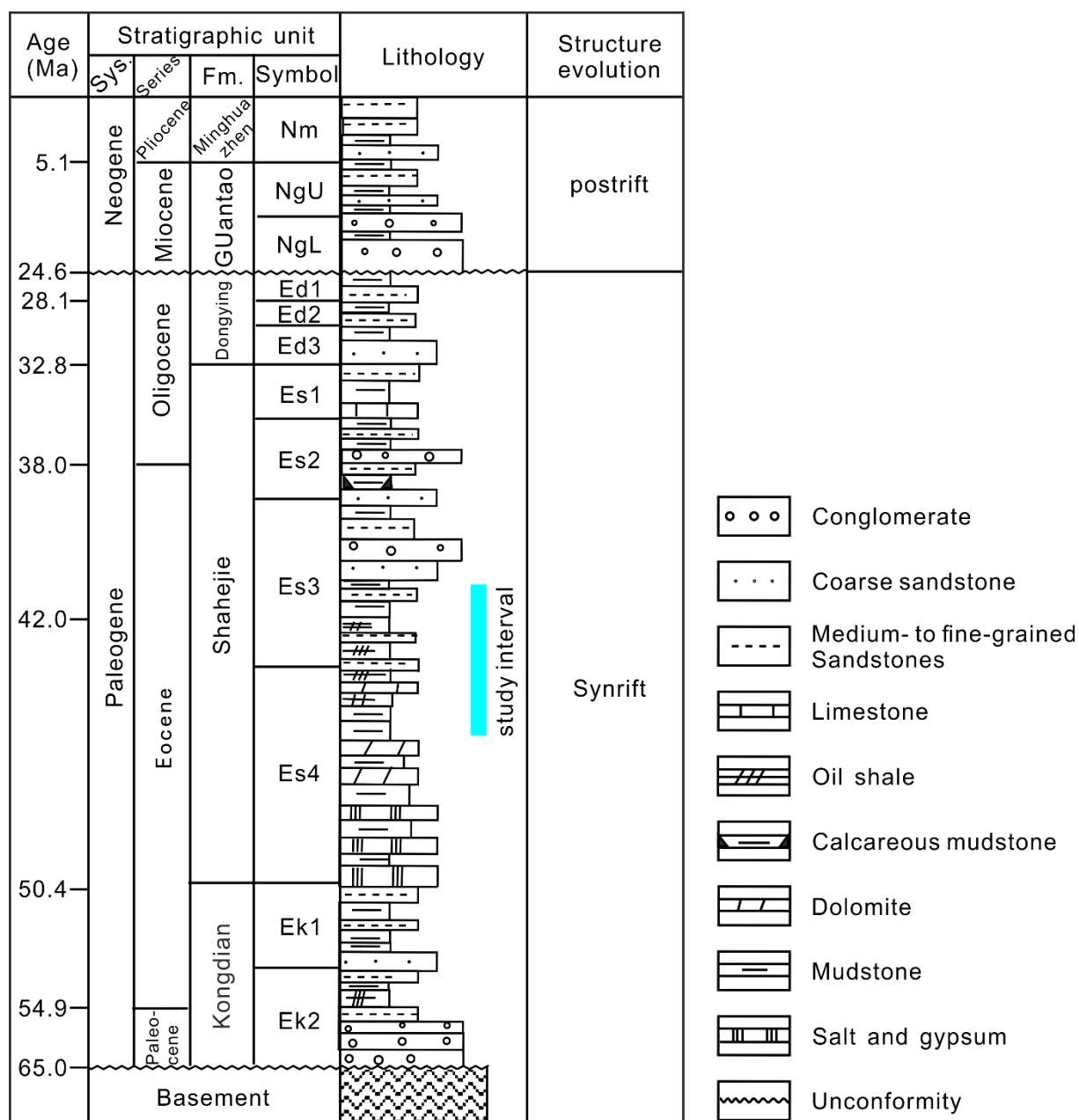


Figure 2. Generalized Cenozoic stratigraphy of the Dongying Sag (modified from [18]). Sys. = System; Fm. = Formation.

3. Data and Methods

3.1. Gamma Ray Well Log Data

The gamma ray (GR) well log reflects the variations in the amount of potassium (K), uranium (U), and thorium (Th) in the rock. Generally speaking, under warm and humid climate conditions, enhanced chemical weathering and runoff will increase the input of clay minerals and organic matter, resulting in higher GR values. On the contrary, cold and arid climate conditions will reduce clay mineral input, resulting in lower GR values [16]. Given the sensitivity of clay mineral and organic matter abundance in lake basins to the environment and climate change, the GR well log can capture the primary signals related to climate variations. In addition, compared with other paleoclimate proxies, it has a relatively high signal-to-noise ratio [21], so it has been widely used in time series analysis [16,22]. In this study, we used the GR records of the Es3L and the Es4U from the wells FY1, LY1, and

NY1 in the Dongying Sag. These wells have continuous GR logging data with a sampling resolution of 0.125 m, which meets the requirements of astronomical analysis.

3.2. Time Series Methods

The potential astronomical–climate signals in GR series within studied successions were identified and interpreted through the following steps: (1) The GR series were detrended by subtracting a 35% weighted average using the LOWESS method to remove the long-term trends [23]. (2) The GR data were analyzed by the 2π multi-taper method (MTM) spectral estimator with robust red noise modeling [24]. Peaks with 90%, 95%, and 99% confidence levels in the spectral analysis graphs were taken into account [25]. (3) In addition, evolutionary fast Fourier transform (FFT) spectrograms were used to study continuous signal variations in frequencies [26], to evaluate the fluctuation in sedimentation rates [27]. (4) Correlation coefficient (COCO) analysis based on Monte Carlo simulations was applied to evaluate the most likely sedimentation rates that yielded the time series that significantly fit given astronomical models. (5) A Gaussian bandpass filter was used to isolate interpreted astronomical parameters. In this study, the La2004 astronomical solution, considered valid over ~ 54 Ma, was used as the astronomical target [28]. Astronomical tuning was used to transform data from the depth domain to the time domain. The 405 kyr long eccentricity is the most stable astronomical parameter in deep time and its longer duration also made it more suitable for the noisy terrestrial stratigraphy. At the same time, tuning using short cycles may have inadvertently missed or double counted cycles. Therefore, the 405 kyr tuning strategy was adopted in this study. All analysis steps were performed using Acycle v2.4 software [29].

3.3. Grayscale Data

High-resolution grayscale data were extracted from the white light slice core scanning photos of the Es3L and Es4U shale by using ImageJTM v1.8.0 software in which 5 mm wide bands were averaged. In this process, the strong meters-to-centimeters scale lithological rhythm was captured, while mass transport beds and core cracks were intentionally avoided as these reflected instantaneous events or artifacts. Since the core photos are separated by each meter, the extracted grayscale data were spliced after the depth correction to obtain the grayscale fluctuation of the entire sequence.

4. Results

4.1. Mineralogy

The Es3L and Es4U shale predominately consists of carbonate minerals (average: 48.84 wt.%), clay minerals (average: 20.51 wt.%), and quartz (average: 23.91 wt.%), with subordinate plagioclase (average: 3.89 wt.%), K-feldspar (average: 0.04 wt.%), pyrite (average: 2.70 wt.%), and anhydrite (average: 0.12 wt.%) (Figure 3A). Calcite is the predominant carbonate with an average content of 38.45 wt.%, followed by dolomite (average: 9.82 wt.%), and a small amount of siderite (average: 0.57 wt.%) (Figure 3A). The ternary diagram of the division of the lithofacies shows that the Es3L and Es4U shale in the Dongying Sag are dominated by calcareous shale and mixed shale, with only a small amount of clay shale and felsic shale (Figure 3B).

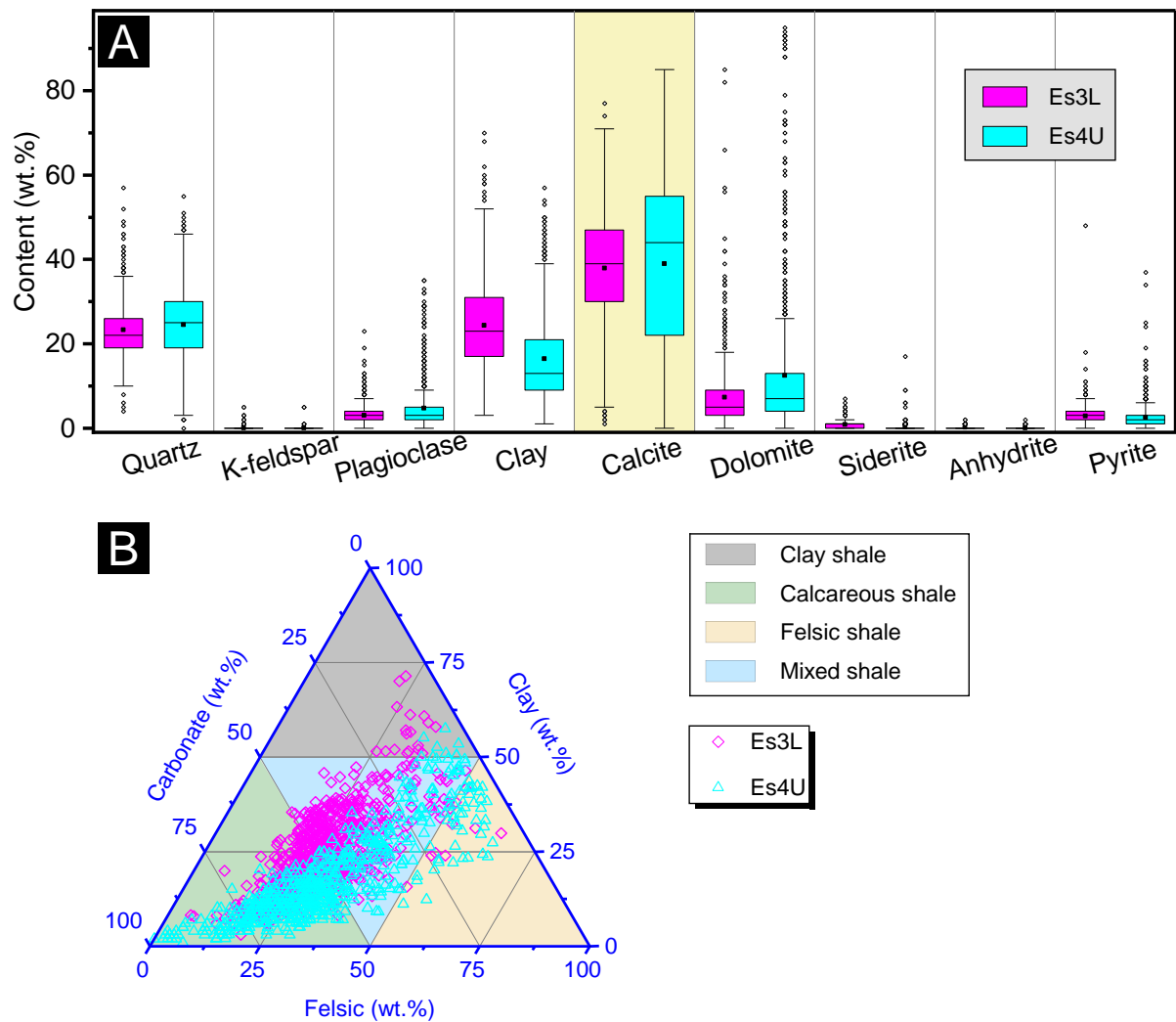


Figure 3. (A) The proportion of main minerals of the Es3L and Es4U shale in the Dongying Sag. (B) Ternary diagram of the division of lithofacies showing that the Es3L and Es4U shale in the Dongying Sag is dominated by calcareous shale and mixed shale, with only a small amount of clay shale and felsic shale.

4.2. Time Series Analysis

Taking well FY1 as an example, the analysis process is described. The MTM power spectrum of the untuned GR profile through the Es3L and Es4U succession in the Dongying Sag has significant peaks (>95% confidence level) at wavelengths of 44.1–30.5 m, 19.4–7.1 m, 5.2–3.2 m, and 2.3–1.6 m (Figure 4). Based on previous studies on the age of strata in the Dongying Sag [30], the theoretical astronomical period of 38–43 Ma was calculated by using the La2004 astronomical solution [28]. The results show that there is a long eccentricity of 405 kyr, short eccentricity of 125 kyr, and 97 kyr, an obliquity of 51 kyr, 40 kyr, 38 kyr, and precession of 28 kyr, 23 kyr, 21 kyr, and 19 kyr, with a ratio between them of about 20:5:2:1, respectively, which is close to the thickness ratio of the above sedimentary cycles. In addition, we utilized evolutionary fast Fourier transform (FFT) spectrograms to inspect the evolution of frequencies through the succession (with a sliding window of 80 m). The results show that the FFT spectrograms show the same frequency as the MTM power spectrum, and the eccentricity signal exists throughout the entire succession, as well as also showing the fluctuation in sedimentation rates (Figure 4).

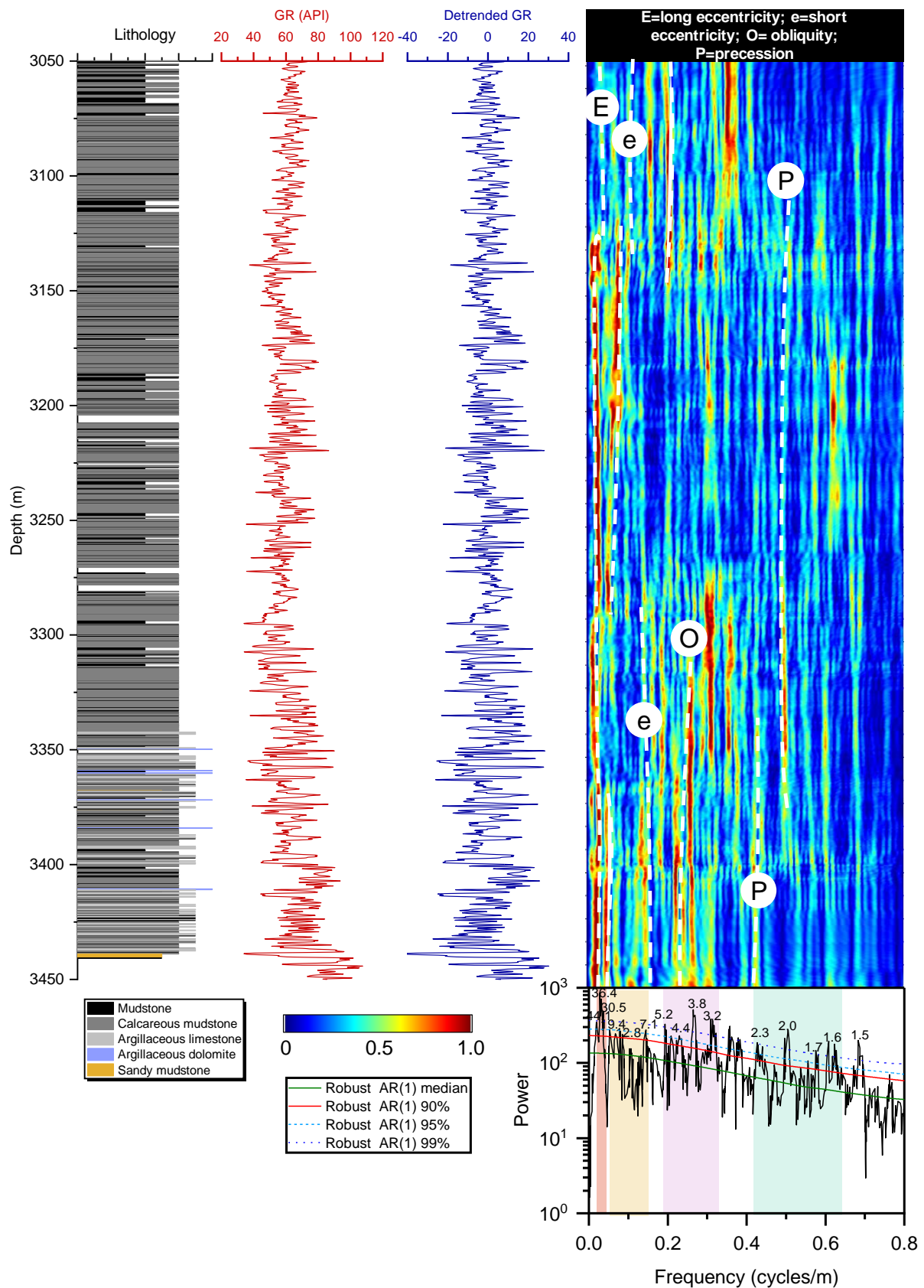


Figure 4. Interpreted cyclostratigraphy from the well FY1 gamma ray (GR) series in the Dongying Sag. Evolutionary power spectra were calculated using an 80 m sliding window. The 2π MTM power spectrum is also shown with a robust AR model and 90%, 95%, and 99% confidence levels.

The MTM power spectrum of the GR series of the Es3L has significant peaks (>95% confidence level) at the wavelengths of 40.8 m, 13.7–9.1 m, 4.8–2.8 m, and 2.3–1.6 m, while the GR series of the Es4U revealed significant sedimentary cycles with wavelengths of 36 m, 17.5–6.9 m, 4.4–3.2 m, and 2.7–1.6 m (Figure 5). The ratios of these wavelength bands are approximately 20:5:2:1, which is consistent with Paleogene theoretical periodicity ratios. To obtain the optimal sedimentation rate for the Es3L and Es4U, a correlation coefficient (COCO) analysis was performed. The number of Monte Carlo simulations was 2000 and the tested sedimentation rates ranged from 0 to 30 cm/kyr with steps of 0.3 cm/kyr. The results show that for the Es3L, there are two main peaks at 10.1 cm/kyr and 12.4 cm/kyr, and it has null hypothesis significance levels lower than 0.001%, with all seven astronomical components involved in the estimation. At the same time, for the Es4U, no orbital signal null hypothesis was rejected at significance levels of below 0.001 at 8.1–9.6 cm/kyr by the involvement of all seven astronomical components (Figure 6). The above estimates of sedimentation rates are close to those of previous studies [31]. Based on the analysis of sedimentation rates, the four cycles of the Es3L and Es4U were considered as a 405 kyr long eccentricity, ~100 kyr short eccentricity, obliquity, and precession cycles, respectively.

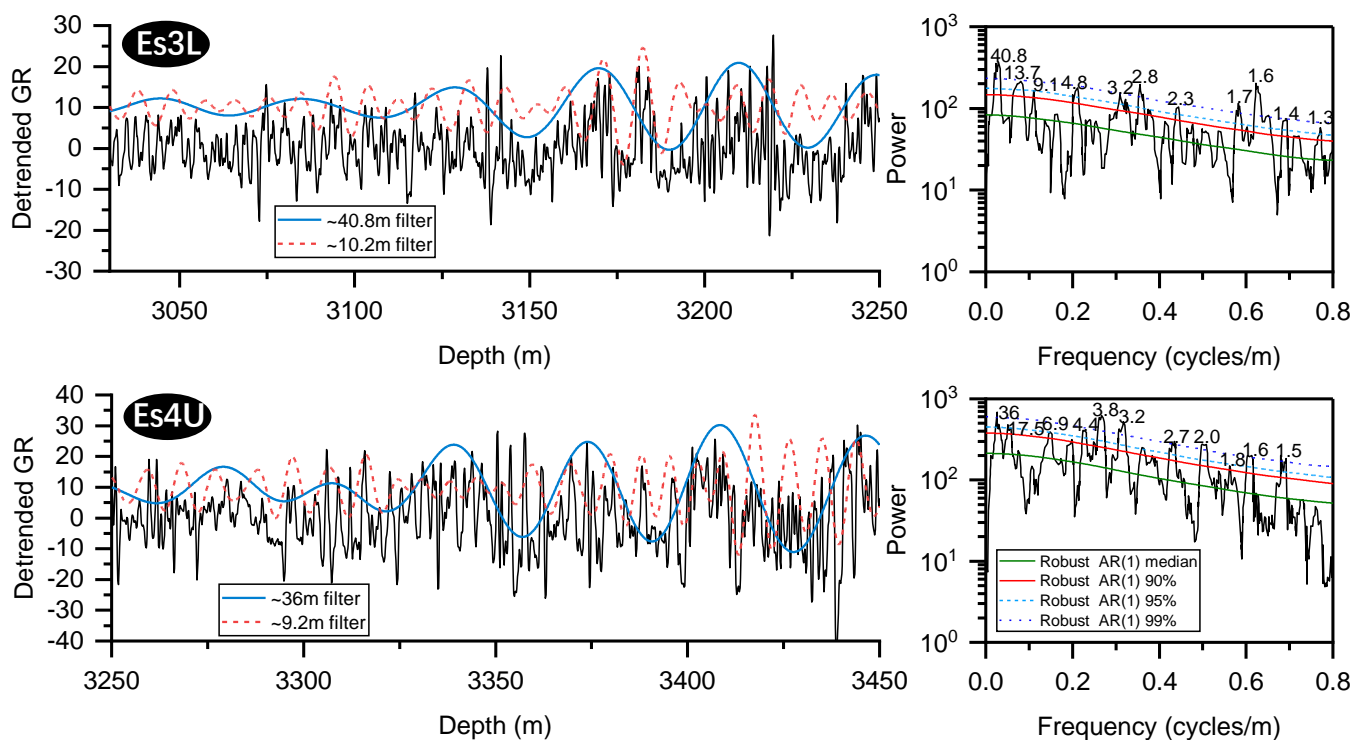


Figure 5. Detrended GR series of the Es3L and Es4U with interpreted long and short eccentricity cycles and an associated 2π MTM power spectrum. GR of Es3L shown with ~40.8 m and ~10.2 m filtered cycles; GR of Es4U shown with ~36.0 m and ~9.2 m filtered cycles.

We filtered the ~40.7 m, ~10.2 m, ~4.2 m, and ~2.1 m cycles of the Es3L and ~36 m, ~9.2 m, ~3.7 m, and ~1.8 m of the Es4U using a Gaussian bandpass filter to identify the long eccentricity, short eccentricity, obliquity, and precession cycles (Figure 5). Given the stability of the 405 kyr cycle, an age model was established with its filtering curve for astronomical tuning, which was performed in Acycle v2.4 software [29]. The above analysis steps were also carried out for well LY1 and well NY1 in the Dongying Sag.

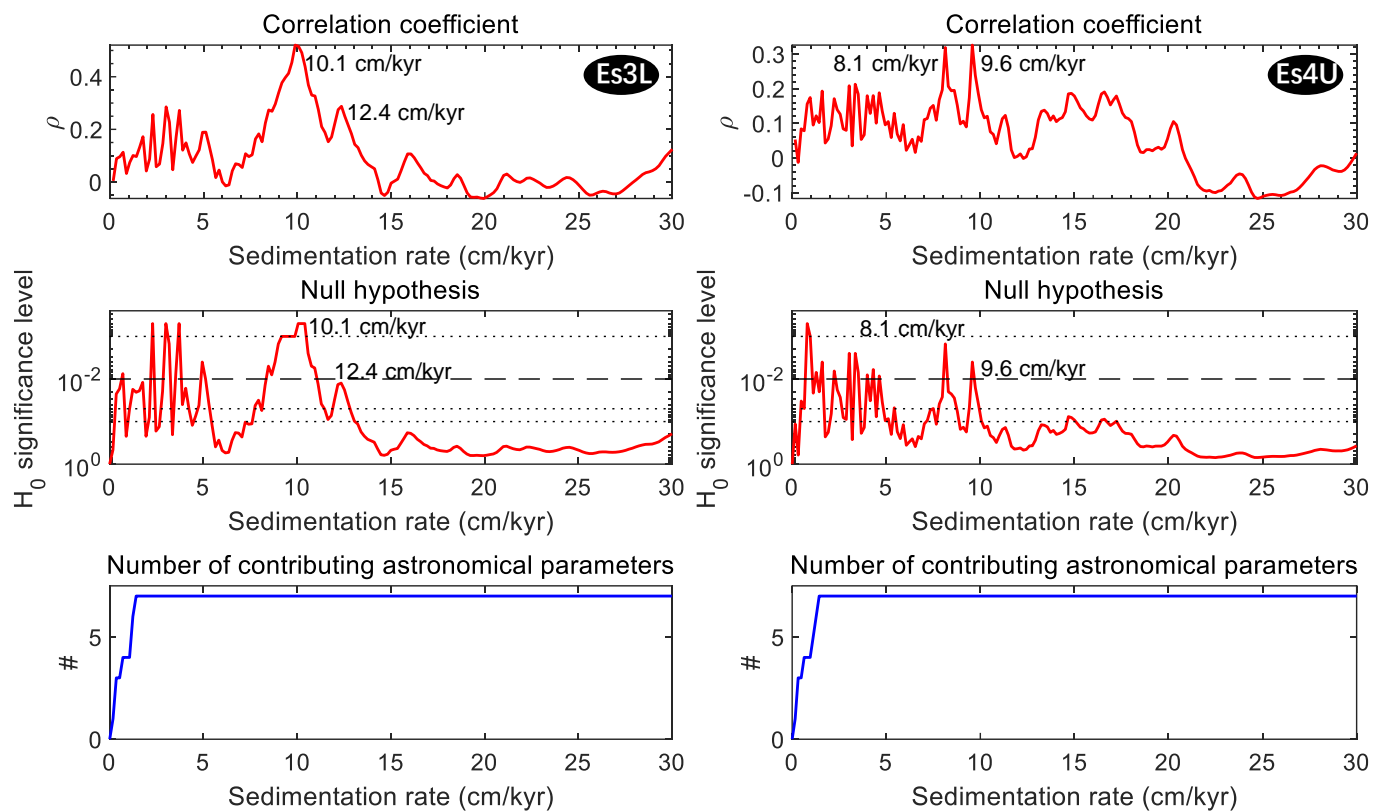


Figure 6. Correlation coefficient (COCO) analysis of the detrended GR series of the Es3L and Es4U. The tested sedimentation rates ranged from 0 to 30 cm/kyr with steps of 0.1 cm/kyr, and the number of Monte Carlo simulation was 2000.

5. Discussion

5.1. Multi-Scale Cyclicity and Astronomical Constraint Interpretation

5.1.1. Hundred-Meter Scale Cyclicity

The Es3L and Es4U in the Dongying Sag include about ~ 10.5 long eccentricity cycles (405 kyr). Accordingly, the Es3L and Es4U can be divided into ~ 11 layers (Layer E1–Layer E11) (Figure 7). At the same time, from the perspective of the duration of the stratigraphic unit, it was roughly estimated to be about 4.2 Ma, which is consistent with the results of Liu et al., 2018 [32], thus verifying the reliability of the results obtained in this study. The variation trend in the TOC value shows that there are two high-value sections, roughly corresponding to Layer E3–Layer E4 and Layer E8–Layer E9 (green box in Figure 7); since the Es3L and Es4U shales contain high carbonate mineral content, the long-term evolution trend of the paleoclimate was reconstructed by a revised CIA, i.e., CIX ($CIX = Al_2O_3 / (Al_2O_3 + Na_2O + K_2O) \times 100$, [33]) and $\ln(Al_2O_3 / Na_2O)$ [34]. The results show that the evolution trend in the paleoclimate could also be divided into four stages (Figure 7).

Therefore, based on the variation in the TOC value and the evolution trend of the paleoclimate, four cycles could be identified in the Es3L and Es4U in the Dongying Sag. The thickness of each cycle is ~ 100 m, and its duration is between ~ 0.8 and 1.2 Ma. It is worth mentioning that Shi et al. also identified four cyclic stages on a single well through the Sr/Ca and V/Cr ratios [31]. It is suggested that the cyclicity of this scale may be controlled by the very long orbital period. Previous studies have shown that climate change driven by the very long orbital period plays an important role in the evolution of lake basins [35]. It is well known that the long period has a modulation effect on the short period [28], so the former could be identified by analyzing the envelope of the latter to prove its existence [36]. An amplitude modulation (AM) analysis could identify the long-term cycles and the specific steps have been described in previous studies [31,36]. Bandpass filtering was performed on the tuned time–domain data to extract the interpreted long eccentricity, short eccentricity,

obliquity, and precession cycles. Then, the AM envelopes were extracted and analyzed by the MTM spectrum. The results show that the AM envelopes of the long eccentricity, short eccentricity, and obliquity show significant spectral peaks corresponding to ~ 1.2 Ma and ~ 0.8 Ma cycles. At the same time, those of the short eccentricity and precession have clear spectral peaks at ~ 405 kyr (Figure 8).

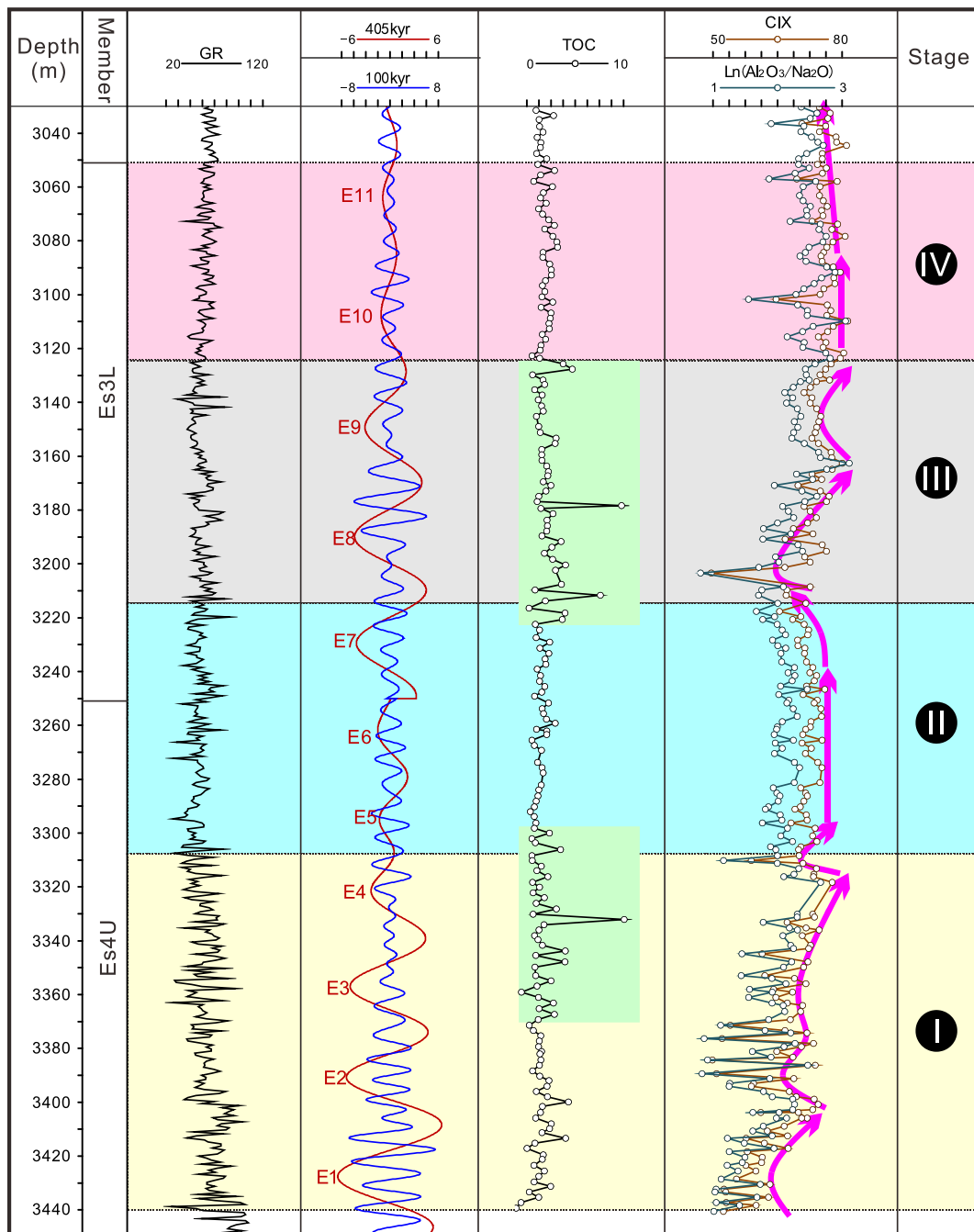


Figure 7. The filtering curves of the eccentricity cycles showing that the Es3L and Es4U in the Dongying Sag include ~ 10.5 long eccentricity cycles. The vertical variation in TOC and weathering proxies showing that the Es3L and Es4U in the Dongying Sag can be divided into four stages. $CIX = Al_2O_3 / (Al_2O_3 + Na_2O + K_2O) \times 100$.

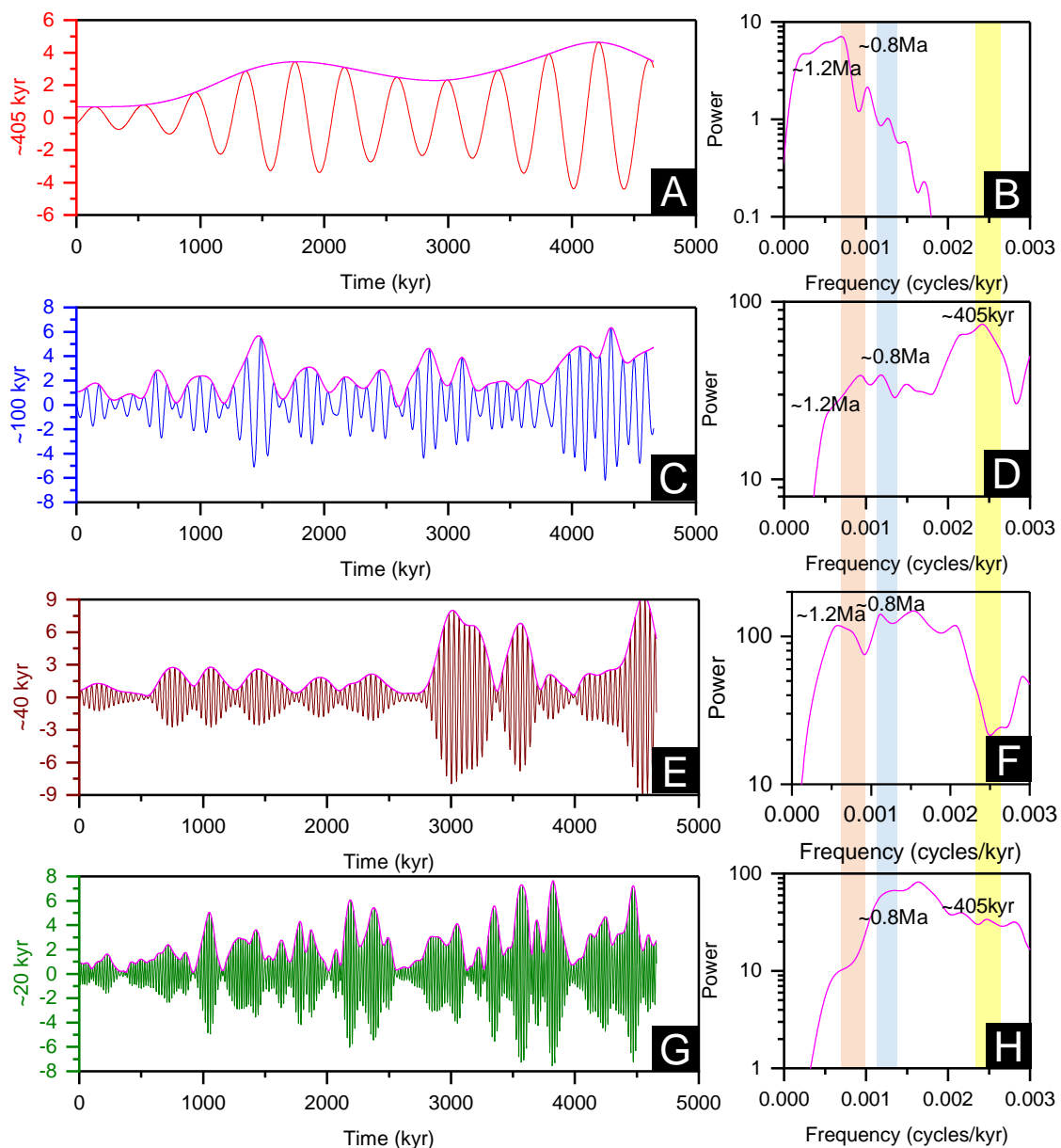


Figure 8. Amplitude modulation (AM) analysis of the 405 kyr long eccentricity, 100 kyr short eccentricity, 40 kyr obliquity, and 20 kyr precession signals. (A,C,E,G) Gaussian filters of the calibrated GR time series. The pink solid lines define the AM envelopes. (B,D,F,H) are 2π MTM power spectra of the AM envelopes shown in (A), (C), (E), and (G), respectively.

The very long orbital period of ~ 1.2 Ma and ~ 0.8 Ma was also identified by magnetic susceptibility series in the Dongying Sag [31]. Studies have shown that the ~ 1.2 Ma cycle is the long period modulation obliquity signal (s_4-s_3) produced by the interaction between the ~ 41 kyr ($p + s_3$) and ~ 39 kyr ($p + s_4$) cycles [28,35,37]. However, the ~ 0.8 Ma cycle was considered to be a unique long period signal in the Dongying Sag [31]. The very long orbital period signals identified by GR logging data in this study undoubtedly further verify the previous research results. The very long orbital period may have a general control effect on the paleoclimate evolution of the Cenozoic. For example, the very long orbital period signal of ~ 1.2 Ma was also found to be stable during the deposition of the Middle Eocene Qianjiang Formation to the Oligocene Jinghezhen Formation in the Jiangnan Basin [38]. At the same time, there are also reports of its existence in the Oligocene and Miocene marine sediments [15,39].

5.1.2. Ten-Meter Scale Cyclicity

High-resolution mineralogical and X-ray fluorescence (XRF) element data show that shale has ten-meter scale cyclicity, and the visual peaks of each parameter match the maxima of 405 kyr long eccentricity. At the same time, the relative contents of Ti, Fe, and Mn reflect the cyclic fluctuation of an arid and humid climate (Figure 9). The multi-taper method (MTM) was applied for the identification of astronomic signals in the TOC, mineralogical, and XRF element data. The results show that almost all the parameters revealed significant sedimentary cycles with wavelengths of ~36 m, ~9 m, ~3.6 m, and ~2 m, which represent the long eccentricity, short eccentricity, obliquity, and precession cycles, respectively (Figure 10). Among them, the long eccentricity and precession cycle signals are the most stable, so they are considered to have strong control over organic matter abundance, mineral composition, and elemental content (Figure 10).

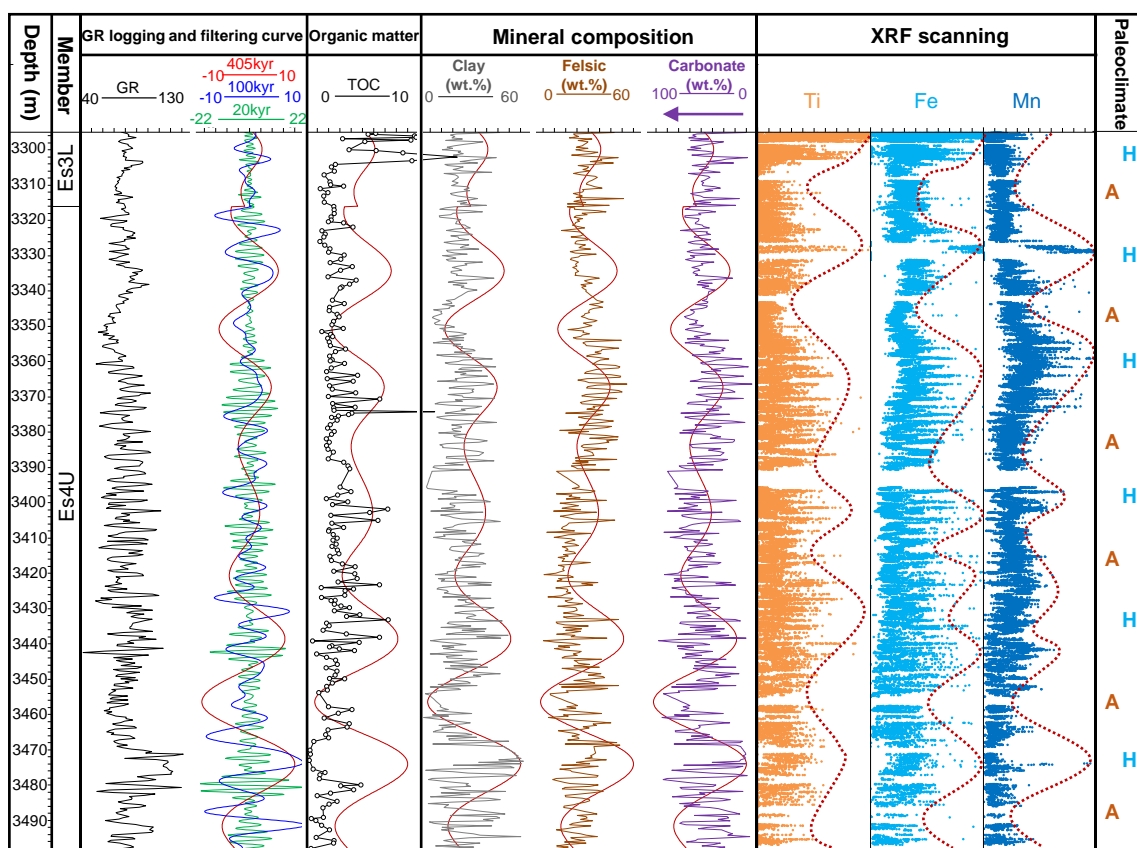


Figure 9. Response characteristics of different geological parameters to long eccentricity cycles. Paleoclimate conditions were mainly inferred based on the relative abundance of elements. XRF = X-ray fluorescence; A = Arid; H = Humid.

Studies have shown that eccentricity actually has little direct effect on solar radiation [40–42], but it can modulate the amplitude of the precession, thereby controlling the seasonal climate differences [28,43]. Figure 9 shows that the amplitude of precession increases near the long eccentricity maxima and vice versa. This phenomenon reflects the modulation effect of the eccentricity on the amplitude of the precession, which is consistent with the results reflected in Figure 8. Therefore, in the vicinity of the long eccentricity maxima, the amplitude of the precession increases, and the seasonal difference in climate is significant [44]. The rainfall in spring and summer increases, and the terrestrial input is higher [45]. With the continuous input of nutrients, the primary productivity increases, and the lake water becomes deeper. These conditions are conducive to the production and preservation of organic matter. In winter and autumn, water temperature decreases, lake

water stratification is stable, and bottom water is anoxic, which is conducive to the preservation of organic matter. At the same time, under the background of higher terrestrial input, the content of clay minerals and felsic minerals increased, while the content of carbonate minerals decreased (Figure 9). When the eccentricity is near the minimum, the amplitude of the precession weakens, and the seasonal difference in climate is not significant. The rainfall in spring and summer is low, the climate is relatively dry, and the terrestrial input decreases. Although the sedimentary environment may be relatively stable at this stage, which is conducive to the preservation of organic matter [41], the organic matter abundance tends to be low due to the limited supply of terrestrial nutrients, which is not conducive to the improvement of lake primary productivity (Figure 9).

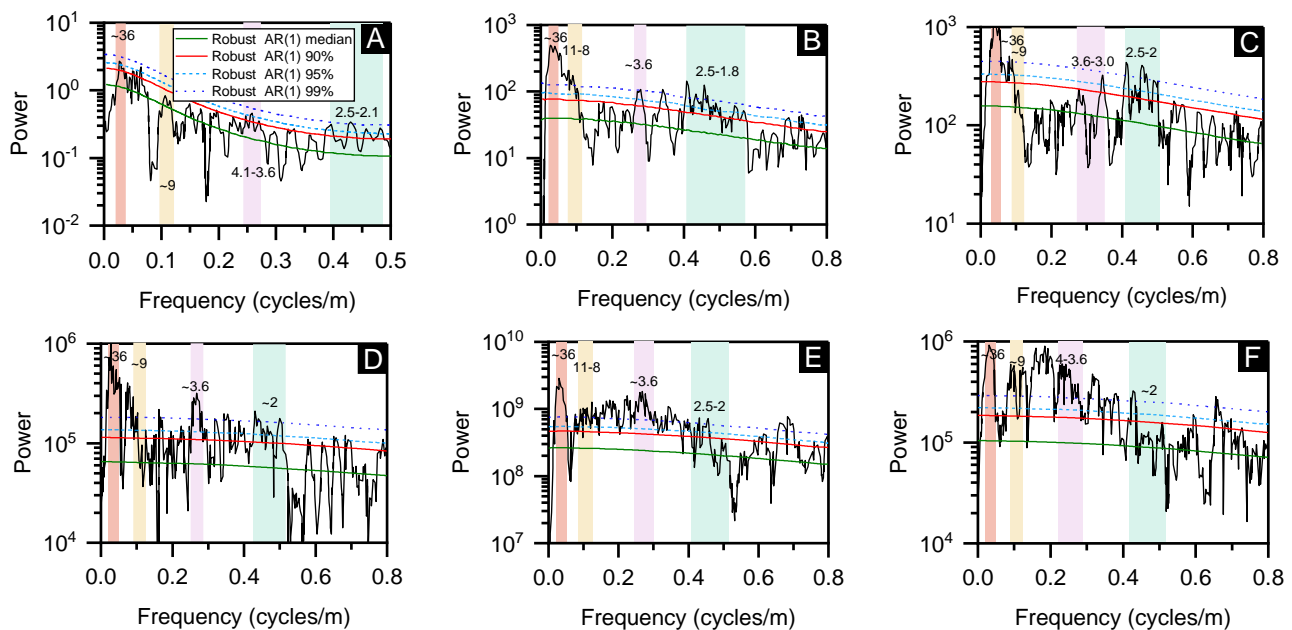


Figure 10. 2π MTM power spectra of different geological parameters with the robust AR model, and 90%, 95%, and 99% confidence levels. (A) TOC content; (B) clay content; (C) carbonate content; (D) relative abundance of Ti; (E) relative abundance of Fe; (F) relative abundance of Mn.

5.1.3. Meter-Scale Cyclicity

Meter-scale cyclicity has been recorded in many basins and various types of sedimentary rocks worldwide [1,3]. The multi-taper method (MTM) spectra show that the TOC, mineralogical, and XRF element data revealed significant sedimentary cycles with wavelengths of ~ 2 m. These meter-scale cycles correspond to the precession period (Figure 10). The insolation difference caused by the precession period can reach 20%, which is considered to significantly affect the climate over various latitudes [46–48]. As for the effect of the precession cycle on climate and lacustrine deposition, previous studies have shown that the climate is warm and humid when the summer is at the perihelion in the precession period [49]; for example, increased annual rainfall [50], increased terrestrial input [51], and expanded vegetation coverage have been observed during this stage [52].

The high-resolution slice core scanning photos of Es3L and Es4U shale in the Dongying Sag show that the dark sections usually have high clay mineral and felsic mineral content, low carbonate mineral content, and the lithofacies are dominated by mixed shale; however, the light sections usually have high carbonate mineral content, low clay mineral and felsic mineral content, and the lithofacies are dominated by calcareous shale (Figure 11). Since the eccentricity has a modulation effect on the precession, a complete long eccentricity period was selected to discuss the sedimentary response to the precession. During the eccentricity maxima, the grayscale value has obvious periodic fluctuation, and the mineral composition and element abundance also have obvious cyclicity. Therefore, the shale has a significant

rhythmicity, reflecting the seasonal enhancement of the climate. The arid and humid fluctuations in climate are frequent and correspond to the precession period (Figure 11); during the eccentricity minima, the grayscale value, various mineral contents, and element abundance are relatively stable. Therefore, the shale does not have significant rhythmicity, reflecting little seasonal variation in climate (Figure 11). In addition, the decrease in the clay and felsic mineral content, the increase in the carbonate mineral content, the decrease in the relative abundance of Ti, Fe, and Mn, and the increase in the relative abundance of Ca all reflect an arid and cold climate during this phase (Figure 11).

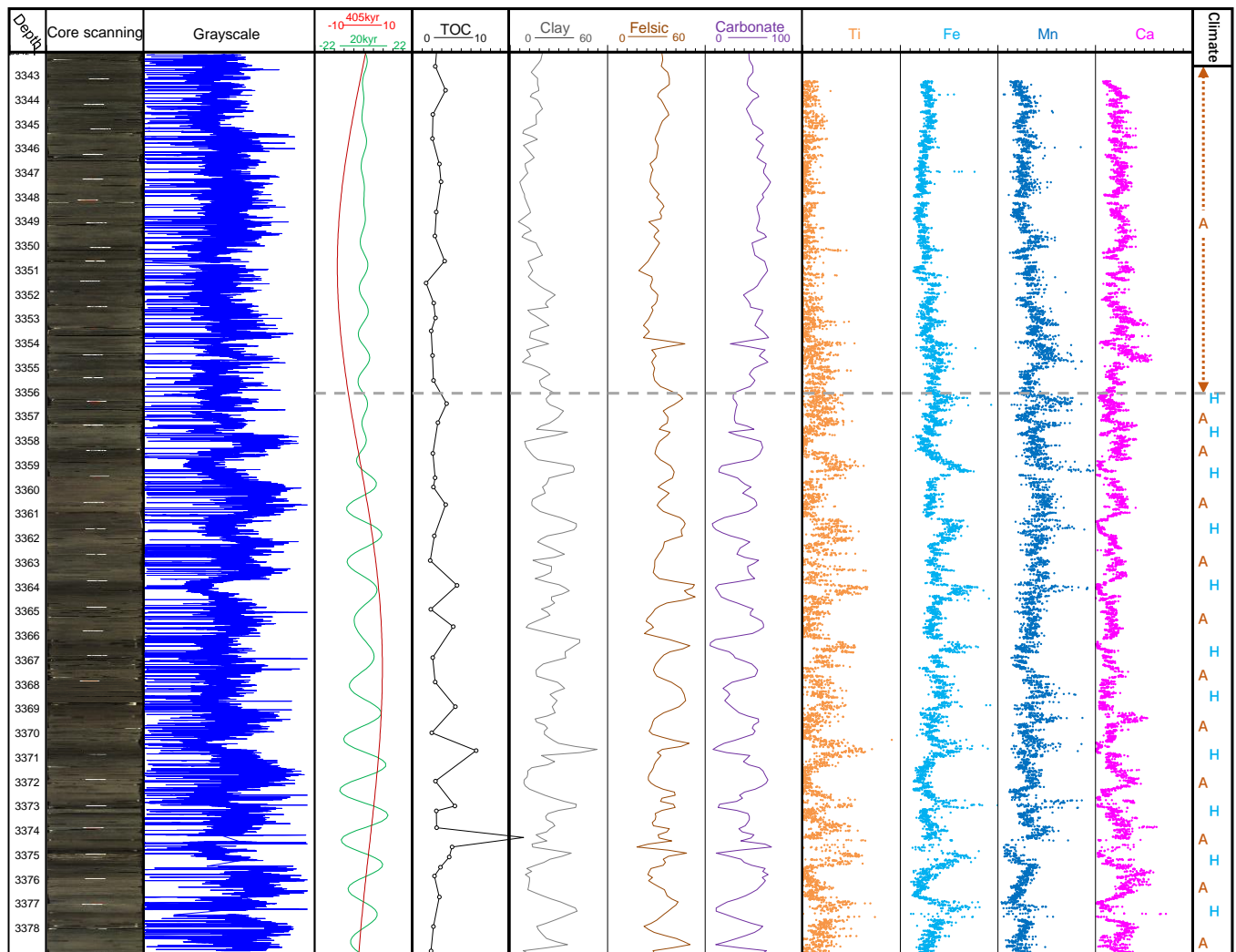


Figure 11. Response characteristics of different geological parameters to precession cycles in a complete long eccentricity cycle. A = Arid; H = Humid.

5.2. A Model of Astronomically Constrained Shale Cyclicality

Lake basins usually have a small scale, which makes them sensitive enough to respond to the insolation changes related to astronomical cycles. Among them, the very long orbital period profoundly affects the long-term evolution of the paleoclimate and controls the general sedimentary environment of the lake at a large scale, which leads to the cyclicality of shale on a hundred-meter scale.

At the same time, eccentricity and precession jointly control the insolation, leading to a paleoclimate that usually varies with the change in their configuration relationship. During the eccentricity minima, Earth's orbit tends to be a perfect circle, and the difference between the perihelion and aphelion becomes smaller. At the same time, the amplitude of the precession is lower. Both of them result in little seasonal variation in climate, with

less rainfall in summer and the generally arid climate during this stage (Hinnov, 2000; Laskar et al., 2004), which makes the shale developed during this stage typically have a higher carbonate mineral content and low clay and felsic mineral content. In addition, nutrient availability is limited as terrestrial input decreases, which is not conducive to the improvement of primary productivity, so the organic matter is usually not enriched (Figure 12A). During the eccentricity maxima, Earth's orbit tends to be elliptical, and the difference between the perihelion and aphelion becomes larger [28,40,49]. At the same time, due to the modulation effect of eccentricity on precession, the amplitude of the precession becomes larger [28,43]. These two factors together contribute to the enhanced seasonality of the climate at this stage. Due to the warm and humid climate in the summer of this stage, the climate was generally humid during the eccentricity maxima, resulting in high clay and felsic mineral content and low carbonate mineral content in the shale developed during this stage. At the same time, due to the high supply of terrestrial nutrients, the organic matter content of shale is relatively high (Figure 12B). Therefore, the difference between the two semi-periods of eccentricity results in the cyclicity of shale on this time scale, and its cyclic thickness usually reaches tens of meters.

In addition, during the eccentricity maxima, due to the high precession amplitude, the seasonal difference in climate in this stage is significant, so it is easy to reach the threshold of sedimentary records, resulting in frequent interbeds of different lithofacies on the meter scale, which is easy to form rhythmic shale; on the contrary, during the eccentricity minima, the lithofacies are relatively simple and it is not easy to form meter-scale cycles. In general, climate change on the orbital time scale profoundly affects the accumulation of organic matter and the vertical stacking characteristics of shales with different lithofacies.

As for the development of shale laminae, it usually requires the periodic repeated supply of different material components. The laminae developed in the Es3L and Es4U shale in the Dongying Sag are generally considered to be annual laminae, formed by the difference in the supply of material components caused by seasonal climate differences. Therefore, for the Northern Hemisphere, during the eccentricity maxima, the seasonal climate differences were enhanced when the perihelion occurred at the summer solstice in the precession period [28,40,49]; in theory, the development degree of shale laminae at this stage should have been higher.

5.3. Implications for Continental Shale Oil Exploration and Development

The vertical heterogeneity of shale reservoirs has an important impact on shale oil exploration and development. Multi-scale cyclicity enables the development of shales with different properties within shale systems, which can be divided into different subunits based on the differences in organic matter abundance and type, lithofacies, petrology, and petrophysics. The differences in these properties will lead to differences in hydrocarbon generation potential, hydrocarbon migration, and accumulation conditions in different subunits. One of our recent studies revealed the migration of hydrocarbons among subunits, which is referred to as "intrasource migration" [53]. The significance for shale oil accumulation is that these subunits constitute a good source–reservoir combination that may ubiquitously exist in shale systems. As for hydraulic fracturing in shale, a weak plane may be formed between these subunits, which affects the mechanical properties of the shale. For example, laminated shales seem to have advantages in reservoir space, oil content and mobility, and fracability. In summary, understanding the controlling factors of shale vertical heterogeneity is crucial for evaluating reservoir properties. This study found that orbital forcing has a dominant control effect on the multi-scale cyclicity of shale, resulting in its vertical heterogeneity, which is of great significance for understanding the genesis of organic-rich shale and predicting high-quality shale reservoirs.

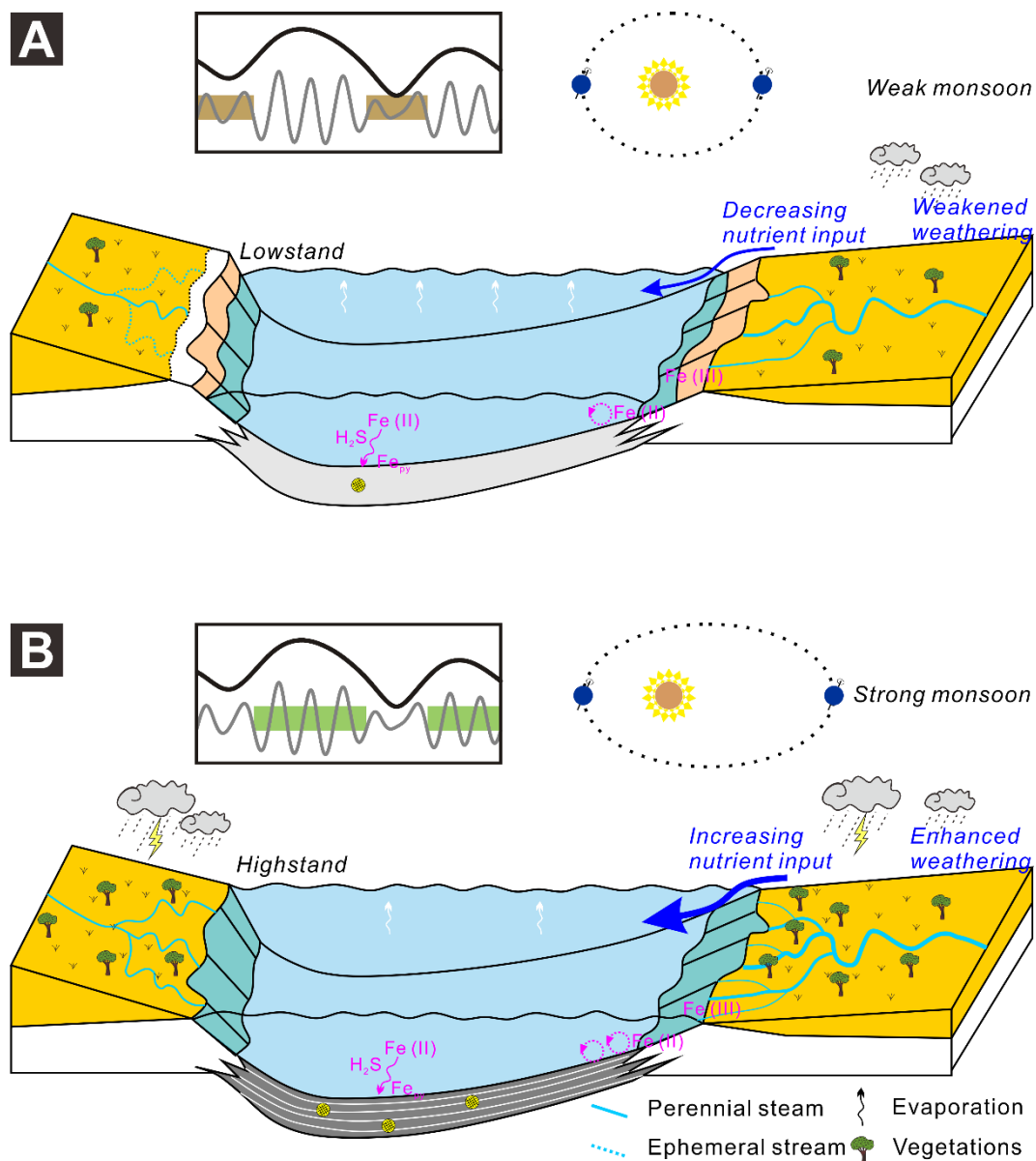


Figure 12. A schematic diagram showing the genesis of astronomically constrained shale cyclicality. (A) During the eccentricity minima, the climatic conditions were characterized as cold and arid with no significant seasonal differences. (B) During the eccentricity maxima, the climatic conditions were characterized as warm and humid with significant seasonal differences (sedimentation pattern diagram modified from [54]).

6. Conclusions

The Es3L and Es4U shale in the Dongying Sag have high carbonate minerals, followed by quartz and clay minerals. The ternary diagram of the division of lithofacies shows that the Es3L and Es4U shale are dominated by calcareous shale and mixed shale, with only a small amount of clay shale and felsic shale.

The Es3L and Es4U shale in the Dongying Sag has multi-scale cyclicality, which is manifested by periodic changes in geological parameters such as organic matter abundance, mineral composition, element abundance, and grayscale. Our present study shows that the cycles on different scales are well coupled with different astronomical periods, suggesting a close relationship between them. The very long orbital period profoundly affects the long-term evolution of the paleoclimate and controls the general sedimentary environment

of the lake at a large scale, ultimately leading to the cyclicity of shale on a hundred-meter scale. The ten-meter scale cyclicity is mainly related to the eccentricity cycle, which is mainly due to the fact that during the eccentricity maxima, the climatic conditions were characterized as warm and humid with significant seasonal differences, while during the eccentricity minima, the climatic conditions were characterized as cold and arid with no significant seasonal differences. The climate differences between these two semi-periods of eccentricity are sufficient to cause the response of the lake system. The precession period is the main driver of the meter-scale cyclicity of the shale.

Due to the modulation effect of eccentricity on precession, the meter-scale cyclicity usually bears the additional imprint of eccentricity forcing, which is mainly manifested in that the meter-scale cyclicity of the shale is not significant during the eccentricity minima, but during the eccentricity maxima, the shale usually has obvious cyclicity on the meter-scale. As for the development of shale laminae, it is speculated that for the Northern Hemisphere, during the eccentricity maxima, the seasonal climate differences were enhanced when the perihelion occurred at the summer solstice in the precession period, but the development degree of the shale laminae in this stage should have been higher.

Author Contributions: Q.L.: conceptualization, methodology, and writing—original draft preparation; S.X.: supervision, writing—review and editing, and validation; J.L.: resources and validation; R.G.: data curation and validation; G.W.: visualization and investigation; Y.W.: software and validation. All authors have read and agreed to the published version of the manuscript.

Funding: This research was supported by the National Natural Science Foundation of China (42122017, 41821002), the Shandong Provincial Key Research and Development Program (2020ZLYS08), and the Special Funds for the Taishan Scholar Project (tsqn202211073).

Data Availability Statement: The data presented in this study are available upon request from the corresponding author.

Conflicts of Interest: The authors declare that they have no financial and personal relationships with other people or organizations that could have inappropriately influenced their work, and there was no professional or other personal interest of any nature or kind in any product, service, and/or company that could be construed as influencing the position presented in the manuscript.

References

1. Eldrett, J.S.; Ma, C.; Bergman, S.C.; Ozkan, A.; Minisini, D.; Lutz, B.; Jactett, S.-J.; Macaulay, C.; Kelly, A.E. Origin of limestone-marlstone cycles: Astronomic forcing of organic-rich sedimentary rocks from the Cenomanian to early Coniacian of the Cretaceous Western Interior Seaway, USA. *Earth Planet. Sci. Lett.* **2015**, *423*, 98–113. [\[CrossRef\]](#)
2. Jaminski, J.; Algeo, T.J.; Maynard, J.B.; Hower, J.C. Climatic origin of dm-scale compositional cyclicity in the Cleveland Member of the Ohio Shale (Upper Devonian), Central Appalachian Basin, USA. *Shales Mudstones* **1998**, *1*, 217–242.
3. Zhang, J.; Jiang, Z.; Liang, C.; Baars, T.F.; Wang, Y.; Abels, H.A. Astronomical forcing of meter-scale organic-rich mudstone–limestone cyclicity in the Eocene Dongying sag, China: Implications for shale reservoir exploration. *AAPG Bull.* **2022**, *106*, 1557–1579. [\[CrossRef\]](#)
4. Kietzmann, D.A.; Palma, R.M.; Llanos, M.P.I. Cyclostratigraphy of an orbitally-driven Tithonian–Valanginian carbonate ramp succession, Southern Mendoza, Argentina: Implications for the Jurassic–Cretaceous boundary in the Neuquén Basin. *Sediment. Geol.* **2015**, *315*, 29–46. [\[CrossRef\]](#)
5. Michalzik, D. Lithofacies, diagenetic spectra and sedimentary cycles of Messinian (Late Miocene) evaporites in SE Spain. *Sediment. Geol.* **1996**, *106*, 203–222. [\[CrossRef\]](#)
6. Westphal, H.; Munneke, A. Limestone-marl alternations: A warm-water phenomenon? *Geology* **2003**, *31*, 263–266. [\[CrossRef\]](#)
7. Li, Q.; Xu, S.; Hao, F.; Shu, Z.; Chen, F.; Lu, Y.; Wu, S.; Zhang, L. Geochemical characteristics and organic matter accumulation of argillaceous dolomite in a saline lacustrine basin: A case study from the paleogene xingouzui formation, Jiangnan Basin, China. *Mar. Pet. Geol.* **2021**, *128*, 105041. [\[CrossRef\]](#)
8. Lu, Y.; Jiang, S.; Lu, Y.; Xu, S.; Shu, Y.; Wang, Y. Productivity or preservation? The factors controlling the organic matter accumulation in the late Katian through Hirnantian Wufeng organic-rich shale, South China. *Mar. Pet. Geol.* **2019**, *109*, 22–35. [\[CrossRef\]](#)
9. Schieber, J.; Southard, J.; Thaisen, K. Accretion of mudstone beds from migrating floccule ripples. *Science* **2007**, *318*, 1760–1763. [\[CrossRef\]](#)
10. Chen, L.; Lu, Y.; Jiang, S.; Li, J.; Guo, T.; Luo, C. Heterogeneity of the Lower Silurian Longmaxi marine shale in the southeast Sichuan Basin of China. *Mar. Pet. Geol.* **2015**, *65*, 232–246. [\[CrossRef\]](#)

11. Hao, F.; Zhou, X.; Zhu, Y.; Yang, Y. Lacustrine source rock deposition in response to co-evolution of environments and organisms controlled by tectonic subsidence and climate, Bohai Bay Basin, China. *Org. Geochem.* **2011**, *42*, 323–339. [[CrossRef](#)]
12. Lourens, L.J.; Antonarakou, A.; Hilgen, F.; Van Hoof, A.; Vergnaud-Grazzini, C.; Zachariasse, W. Evaluation of the Plio-Pleistocene astronomical timescale. *Paleoceanography* **1996**, *11*, 391–413. [[CrossRef](#)]
13. Strasser, A.; Hilgen, F.J.; Heckel, P.H. Cyclostratigraphy—concepts, definitions, and applications. *Newsl. Stratigr.* **2006**, *42*, 75–114. [[CrossRef](#)]
14. Hays, J.D.; Imbrie, J.; Shackleton, N.J. Variations in the Earth's Orbit: Pacemaker of the Ice Ages: For 500,000 years, major climatic changes have followed variations in obliquity and precession. *Science* **1976**, *194*, 1121–1132. [[CrossRef](#)]
15. Palike, H.; Norris, R.D.; Herrle, J.O.; Wilson, P.A.; Coxall, H.K.; Lear, C.H.; Shackleton, N.J.; Tripathi, A.K.; Wade, B.S. The heartbeat of the Oligocene climate system. *Science* **2006**, *314*, 1894–1898. [[CrossRef](#)]
16. Wu, H.; Zhang, S.; Hinnov, L.A.; Jiang, G.; Yang, T.; Li, H.; Wan, X.; Wang, C. Cyclostratigraphy and orbital tuning of the terrestrial upper Santonian–Lower Danian in Songliao Basin, northeastern China. *Earth Planet. Sci. Lett.* **2014**, *407*, 82–95. [[CrossRef](#)]
17. Webber, A.J. High-resolution faunal gradient analysis and an assessment of the causes of meter-scale cyclicity in the type Cincinnati Series (Upper Ordovician). *Palaaios* **2002**, *17*, 545–555. [[CrossRef](#)]
18. Feng, Y.; Li, S.; Lu, Y. Sequence stratigraphy and architectural variability in late Eocene lacustrine strata of the Dongying Depression, Bohai Bay Basin, eastern China. *Sediment. Geol.* **2013**, *295*, 1–26. [[CrossRef](#)]
19. Hao, F.; Zhou, X.; Zhu, Y.; Zou, H.; Bao, X.; Kong, Q. Mechanisms of petroleum accumulation in the Bozhong sub-basin, Bohai Bay Basin, China. Part 1: Origin and occurrence of crude oils. *Mar. Pet. Geol.* **2009**, *26*, 1528–1542.
20. Liu, H.; Zhang, S.; Song, G.; Xuejun, W.; Teng, J.; Wang, M.; Bao, Y.; Yao, S.; Wang, W.; Zhang, S. Effect of shale diagenesis on pores and storage capacity in the Paleogene Shahejie Formation, Dongying Depression, Bohai Bay Basin, east China. *Mar. Pet. Geol.* **2019**, *103*, 738–752. [[CrossRef](#)]
21. Li, M.; Huang, C.; Ogg, J.; Zhang, Y.; Hinnov, L.; Wu, H.; Chen, Z.-Q.; Zou, Z. Paleoclimate proxies for cyclostratigraphy: Comparative analysis using a Lower Triassic marine section in South China. *Earth-Sci. Rev.* **2019**, *189*, 125–146. [[CrossRef](#)]
22. Huang, C.; Hinnov, L. Astronomically forced climate evolution in a saline lake record of the middle Eocene to Oligocene, Jiangnan Basin, China. *Earth Planet. Sci. Lett.* **2019**, *528*, 115846. [[CrossRef](#)]
23. Cleveland, W.S. Robust locally weighted regression and smoothing scatterplots. *J. Am. Stat. Assoc.* **1979**, *74*, 829–836. [[CrossRef](#)]
24. Thomson, D.J. Spectrum estimation and harmonic analysis. *Proc. IEEE* **1982**, *70*, 1055–1096. [[CrossRef](#)]
25. Mann, M.E.; Lees, J.M. Robust estimation of background noise and signal detection in climatic time series. *Clim. Chang.* **1996**, *33*, 409–445. [[CrossRef](#)]
26. Kodama, K.P.; Hinnov, L.A. *Rock Magnetic Cyclostratigraphy*; John Wiley & Sons: New York, NY, USA, 2014; Volume 5.
27. Li, M.; Kump, L.R.; Hinnov, L.A.; Mann, M.E. Tracking variable sedimentation rates and astronomical forcing in Phanerozoic paleoclimate proxy series with evolutionary correlation coefficients and hypothesis testing. *Earth Planet. Sci. Lett.* **2018**, *501*, 165–179. [[CrossRef](#)]
28. Laskar, J.; Robutel, P.; Joutel, F.; Gastineau, M.; Correia, A.; Levrard, B. A long-term numerical solution for the insolation quantities of the Earth. *Astron. Astrophys.* **2004**, *428*, 261–285. [[CrossRef](#)]
29. Li, M.; Hinnov, L.; Kump, L. Acycle: Time-series analysis software for paleoclimate research and education. *Comput. Geosci.* **2019**, *127*, 12–22. [[CrossRef](#)]
30. Yao, Y.; Xu, D.; Zhang, H.; Han, Y.; Zhang, S.; Yin, Z.; Li, B.; He, Q.; Bian, X. A brief introduction to the Cenozoic astrostratigraphic time scale for the Dongying Depression, Shandong. *J. Stratigr.* **2007**, *31* (Suppl. 2), 423–429.
31. Shi, J.; Jin, Z.; Liu, Q.; Huang, Z.; Hao, Y. Terrestrial sedimentary responses to astronomically forced climate changes during the Early Paleogene in the Bohai Bay Basin, eastern China. *Palaeoogeogr. Palaeoclimatol. Palaeoecol.* **2018**, *502*, 1–12. [[CrossRef](#)]
32. Liu, Z.; Huang, C.; Algeo, T.J.; Liu, H.; Hao, Y.; Du, X.; Lu, Y.; Chen, P.; Guo, L.; Peng, L. High-resolution astrochronological record for the Paleocene–Oligocene (66–23 Ma) from the rapidly subsiding Bohai Bay Basin, northeastern China. *Palaeoogeogr. Palaeoclimatol. Palaeoecol.* **2018**, *510*, 78–92. [[CrossRef](#)]
33. Garzanti, E.; Vermeesch, P.; Padoan, M.; Resentini, A.; Vezzoli, G.; Andò, S. Provenance of passive-margin sand (Southern Africa). *J. Geol.* **2014**, *122*, 17–42. [[CrossRef](#)]
34. von Eynatten, H.; Barceló-Vidal, C.; Pawlowsky-Glahn, V. Modelling compositional change: The example of chemical weathering of granitoid rocks. *Math. Geol.* **2003**, *35*, 231–251. [[CrossRef](#)]
35. Abels, H.A.; Aziz, H.A.; Krijgsman, W.; Smeets, S.J.; Hilgen, F.J. Long-period eccentricity control on sedimentary sequences in the continental Madrid Basin (middle Miocene, Spain). *Earth Planet. Sci. Lett.* **2010**, *289*, 220–231. [[CrossRef](#)]
36. Fang, Q.; Wu, H.; Hinnov, L.A.; Jing, X.; Wang, X.; Yang, T.; Li, H.; Zhang, S. Astronomical cycles of Middle Permian Maokou Formation in South China and their implications for sequence stratigraphy and paleoclimate. *Palaeoogeogr. Palaeoclimatol. Palaeoecol.* **2017**, *474*, 130–139. [[CrossRef](#)]
37. Zachos, J.; Pagani, M.; Sloan, L.; Thomas, E.; Billups, K. Trends, rhythms, and aberrations in global climate 65 Ma to present. *Science* **2001**, *292*, 686–693. [[CrossRef](#)] [[PubMed](#)]
38. Huang, C.; Hinnov, L.A. Evolution of an Eocene–Oligocene saline lake depositional system and its controlling factors, Jiangnan Basin, China. *J. Earth Sci.* **2014**, *25*, 959–976. [[CrossRef](#)]

39. Lirer, F.; Harzhauser, M.; Pelosi, N.; Piller, W.E.; Schmid, H.P.; Sprovieri, M. Astronomically forced teleconnection between Paratethyan and Mediterranean sediments during the Middle and Late Miocene. *Palaeogeogr. Palaeoclimatol. Palaeoecol.* **2009**, *275*, 1–13. [[CrossRef](#)]
40. Berger, A. Milankovitch theory and climate. *Rev. Geophys.* **1988**, *26*, 624–657. [[CrossRef](#)]
41. Gambacorta, G.; Menichetti, E.; Trincianti, E.; Torricelli, S. Orbital control on cyclical primary productivity and benthic anoxia: Astronomical tuning of the Telychian Stage (Early Silurian). *Palaeogeogr. Palaeoclimatol. Palaeoecol.* **2018**, *495*, 152–162. [[CrossRef](#)]
42. Imbrie, J.; Berger, A.; Boyle, E.; Clemens, S.; Duffy, A.; Howard, W.; Kukla, G.; Kutzbach, J.; Martinson, D.; McIntyre, A. On the structure and origin of major glaciation cycles 2. The 100,000-year cycle. *Paleoceanography* **1993**, *8*, 699–735. [[CrossRef](#)]
43. Hinnov, L.A. New perspectives on orbitally forced stratigraphy. *Annu. Rev. Earth Planet. Sci.* **2000**, *28*, 419–475. [[CrossRef](#)]
44. Wang, P.; Wang, B.; Cheng, H.; Fasullo, J.; Guo, Z.; Kiefer, T.; Liu, Z. The global monsoon across timescales: Coherent variability of regional monsoons. *Clim. Past* **2014**, *10*, 2007–2052. [[CrossRef](#)]
45. Ma, W.; Tian, J.; Li, Q.; Wang, P. Simulation of long eccentricity (400-kyr) cycle in ocean carbon reservoir during Miocene Climate Optimum: Weathering and nutrient response to orbital change. *Geophys. Res. Lett.* **2011**, *38*, 1–5. [[CrossRef](#)]
46. Berger, A.; Loutre, M.-F.; Laskar, J. Stability of the astronomical frequencies over the Earth's history for paleoclimate studies. *Science* **1992**, *255*, 560–566. [[CrossRef](#)]
47. Spicer, R.A.; Yang, J.; Herman, A.B.; Kodrul, T.; Maslova, N.; Spicer, T.E.; Aleksandrova, G.; Jin, J. Asian Eocene monsoons as revealed by leaf architectural signatures. *Earth Planet. Sci. Lett.* **2016**, *449*, 61–68. [[CrossRef](#)]
48. Thomson, D.J. The seasons, global temperature, and precession. *Science* **1995**, *268*, 59–68. [[CrossRef](#)]
49. Hinnov, L.A. Cyclostratigraphy and its revolutionizing applications in the earth and planetary sciences. *GSA Bull.* **2013**, *125*, 1703–1734. [[CrossRef](#)]
50. Abels, H.A.; Abdul Aziz, H.; Calvo, J.P.; Tuenter, E. Shallow lacustrine carbonate microfacies document orbitally paced lake-level history in the Miocene Teruel Basin (North-East Spain). *Sedimentology* **2009**, *56*, 399–419. [[CrossRef](#)]
51. Sierro, F.J.; Ledesma, S.; Flores, J.-A.; Torrecusa, S.; del Olmo, W.M. Sonic and gamma-ray astrochronology: Cycle to cycle calibration of Atlantic climatic records to Mediterranean sapropels and astronomical oscillations. *Geology* **2000**, *28*, 695–698. [[CrossRef](#)]
52. Magri, D.; Tzedakis, P. Orbital signatures and long-term vegetation patterns in the Mediterranean. *Quat. Int.* **2000**, *73*, 69–78. [[CrossRef](#)]
53. Li, Q.; Chen, F.; Wu, S.; Zhang, L.; Wang, Y.; Xu, S. A simple and effective evaluation method for lacustrine shale oil based on mass balance calculation of Rock-Eval data. *Appl. Geochem.* **2022**, *140*, 105287. [[CrossRef](#)]
54. Ma, Y.; Fan, M.; Lu, Y.; Liu, H.; Hao, Y.; Xie, Z.; Liu, Z.; Peng, L.; Du, X.; Hu, H. Climate-driven paleolimnological change controls lacustrine mudstone depositional process and organic matter accumulation: Constraints from lithofacies and geochemical studies in the Zhanhua Depression, eastern China. *Int. J. Coal Geol.* **2016**, *167*, 103–118. [[CrossRef](#)]

Disclaimer/Publisher's Note: The statements, opinions and data contained in all publications are solely those of the individual author(s) and contributor(s) and not of MDPI and/or the editor(s). MDPI and/or the editor(s) disclaim responsibility for any injury to people or property resulting from any ideas, methods, instructions or products referred to in the content.